[Supporting information]

Experimental

All solvents were purchased as reagent grade and used without further purification. All the synthetic reactions were carried out under aerobic conditions.

(a) Preparation of $[1a]Cl_2$ and $[1b]Cl_2$.

To a suspension of *fac*-$[Rh(aet)_3]$ [6a] (0.30 g, 0.90 mmol) in DMF (20 cm^3) was added 2,2'-bis(bromomethyl)-1,1'-biphenyl (0.33 g, 0.98 mmol). The mixture was stirred at 40 °C for 4 hours, during which time the suspension became a clear red-orange solution. The red-orange solution was treated with diethyl ether several times to extract DMF. The remaining yellow solid was dissolved in water and then poured onto an SP-Sephadex C-25 column (3 × 30 cm, Na^+ form). After the column had been washed with water, two clearly separated orange bands of $\Delta SS(S_{ax})/\Lambda RR(R_{ax})$-$[Rh(aet)(L)]^{2+}$ ($[\mathbf{1a}]^{2+}$) and $\Delta SS(R_{ax})/\Lambda RR(S_{ax})$-$[Rh(aet)(L)]^{2+}$ ($[\mathbf{1b}]^{2+}$) (L = 2,2'-bis(2-aminoethylthio-methyl)-1,1'-biphenyl) were eluted with a 0.15 mol dm^{-3} aqueous solution of NaCl. The formation ratio of $[\mathbf{1a}]^{2+}$:$[\mathbf{1b}]^{2+}$ was estimated to be ca. 1:2, based on the absorption spectral measurements of the eluates.

These two bands were concentrated to a small volume with a rotary evaporator and desalted by adding ethanol. Each of the resulting orange solution was concentrated to a small volume, followed by the addition of a saturated aqueous solution of NaCl to give orange crystals suitable for X-ray analysis. Yield for $[\mathbf{1a}]Cl_2{\cdot}5H_2O$: 0.07 g (12 % based on *fac*-$[Rh(aet)_3]$). Anal. Calcd for $[Rh(C_2H_6NS)(C_{18}H_{24}N_2S_2)]Cl_2{\cdot}5H_2O$: C, 35.72; H, 5.99; N, 6.25%. Found: C, 35.72; H, 5.74; N, 6.29%. Molar conductivity in water: 241.2 Ω^{-1} cm^2 mol^{-1}. ^1H NMR (D_2O, ppm from DSS = Sodium 2,2-dimethyl-2-silapentane-5-sulfonato) δ 7.56-7.52 (*m*, 5H), 7.41-7.40 (*m*, 2H), 7.12 (*d*, *J* = 6.7 Hz, 1H), 4.62 (*d*, *J* = 13.4 Hz, 1H), 4.25 (*d*, *J* = 14.0 Hz, 1H), 4.11 (*d*, *J* = 14.7 Hz, 1H), 3.98 (*d*, *J* = 14.0 Hz, 1H), 3.22-3.17 (*m*, 4H), 2.95-2.88 (*m*, 4H), 2.73-2.61 (*m*, 2H), 2.40-2.34 (*m*, 1H), 1.96 (*dt*, *J* = 13.2 Hz, 3.5 Hz). $^{13}C\{^1H\}$ NMR (D_2O, ppm from DSS) δ 144.4, 141.6, 136.0, 134.8, 133.8, 133.2, 133.0, 132.6, 131.7, 131.4, 130.6, 52.2, 46.6, 44.6, 44.1, 42.6, 41.2, 37.4, 31.8. ESI-MS (in $MeOH/H_2O$) *m*/*z*: 255.5 ($[M]^{2+}$/ 100 %), 510.0 ($[M-H]^+$/ 40.2 %).

Yield for $[\mathbf{1b}]Cl_2{\cdot}H_2O$: 0.17 g (31 % based on *fac*-$[Rh(aet)_3]$). Anal. Calcd for $[Rh(C_2H_6NS)(C_{18}H_{24}N_2S_2)]Cl_2{\cdot}H_2O$: C, 40.00; H, 5.37; N, 7.00%. Found: C, 39.95; H,

5.23; N, 7.03%. Molar conductivity in water: 230.7 Ω^{-1} cm^2 mol^{-1}. ^1H NMR (D_2O, ppm from DSS) δ 7.91 (*d*, *J* = 7.9 Hz, 1H), 7.70 (*d*, *J* = 7.9 Hz, 1H), 7.57 (*t*, *J* = 7.6 Hz, 1H), 7.52 (*t*, *J* = 7.6 Hz, 1H), 7.48 (*t*, *J* = 7.6 Hz, 1H), 7.45 (*t*, *J* = 7.3 Hz, 1H), 7.16 (*d*, *J* = 7.9 Hz, 1H), 7.11 (*d*, *J* = 7.6 Hz, 1H), 4.43 (*d*, *J* = 12.2 Hz, 1H), 4.35 (*d*, *J* = 13.4 Hz, 1H), 3.96 (*d*, *J* = 14.0 Hz, 1H), 3.81 (*d*, *J* = 13.4 Hz, 1H), 3.39-3.34 (*m*, 1H), 3.28-3.15 (*m*, 4H), 3.10-3.09 (*m*, 3H), 2.99-2.89 (*m*, 2H), 2.38-2.33 (*m*, 1H), 2.16 (*ddd*, *J* = 13.0, 6.3, 4.1 Hz, 1H). $^{13}C\{^1H\}$ NMR (D_2O, ppm from DSS) 142.3, 141.9, 133.4, 133.3, 132.8, 132.52, 132.47, 131.9, 131.5, 131.0, 130.9, 54.6, 47.9, 46.4, 45.4, 44.5, 43.5, 42.9, 32.0. ESI-MS (in MeOH/H_2O) *m*/*z*: 255.5 ($[M]^{2+}$/ 100 %), 510.0 ($[M\text{-}H]^+$/ 25.8 %).

(b) Optical resolution of Δ*SS*(*S*$_{ax}$)/Λ*RR*(*R*$_{ax}$)-[Rh(aet)(L)]$^{2+}$ ([1a]$^{2+}$).

An aqueous solution of [**1a**]Cl_2 was chromatographed on an SP-Sephadex C-25 column (Na^+ form, 3 × 120 cm), using a 0.08 mol dm^{-3} aqueous solution of $Na_2[Sb_2((R,R)\text{-tartrato})_2]\cdot 5H_2O$ as an eluent. When the developed band was broadly separated into two bands in the column, the eluent was changed to a 0.15 mol dm^{-3} aqueous solution of NaCl after sweeping with water. Each eluate was fractionated in portions of *ca*. 100 cm^3 each. Each fraction was concentrated to a small volume with a rotary evaporator, which was used for the CD spectral measurements. The concentration of each eluate was evaluated from the absorption spectral data of the racemic chloride salt of [**1a**]$^{2+}$. It was found from the absorption and the CD spectral measurements that the earlier and the later several fractions contained the pure $(+)_{330}^{CD}$ and $(-)_{330}^{CD}$ isomers, respectively.

(c) Optical resolution of Δ*SS*(*R*$_{ax}$)/Λ*RR*(*S*$_{ax}$)-[Rh(aet)(L)]$^{2+}$ ([1b]$^{2+}$).

The complex [**1b**]Cl_2 was also optically resolved by the same column chromatographic procedure. It was found from the absorption and the CD spectral measurements that the earlier and the later fractions contained the pure $(-)_{330}^{CD}$ and $(+)_{330}^{CD}$ isomers, respectively.

(d) The reaction of Δ-[Rh(aet)$_3$] with 2,2'-bis(bromomethyl-1,1'-biphenyl.

To a suspension of Δ-[Rh(aet)$_3$] [6b,c] (0.18 g, 0.54 mmol) in DMF (18 cm^3) was added

2,2’-bis(bromomethyl)-1,1’-biphenyl (0.20 g, 0.59 mmol). The mixture was stirred at room temperature for 12 h, during which time the suspension became a clear red-orange solution. The red-orange solution was treated with diethyl ether several times to extract DMF. The remaining yellow solid was dissolved in water and then poured onto an SP-Sephadex C-25 column (3 × 40 cm, Na^+ form). After the column had been washed with water, two clearly separated orange bands of $\Delta SS(S_{ax})$-$[Rh(aet)(L)]^{2+}$ ($(-)^{CD}_{330}$-$[\mathbf{1a}]^{2+}$) and $\Delta SS(R_{ax})$-$[Rh(aet)(L)]^{2+}$ ($(-)^{CD}_{330}$-$[\mathbf{1b}]^{2+}$) were eluted with a 0.15 mol dm^{-3} aqueous solution of NaCl. These two bands were concentrated to a small volume with a rotary evaporator, which was used for the absorption and CD spectral measurements. The formation ratio of $(-)^{CD}_{330}$-$[\mathbf{1a}]^{2+}$:$(-)^{CD}_{330}$-$[\mathbf{1b}]^{2+}$ was estimated to be ca. 1:2, based on the absorption spectral measurements of the eluates.

X-ray crystal structure determination.

Single crystal X-ray diffraction measurements for $[\mathbf{1a}]Cl_2 \cdot 4.35H_2O$ were made on a Rigaku RAXIS-RAPID imaging plate area detector with a graphite monochrometed Mo-Kα radiation. Unit cell parameters were determined by a least-squares refinement, using the 93261 reflections. A total of 73 oscillation images were collected. A sweep of data was done using ω scan mode up to $2\theta = 55.0°$. An empirical absorption correction was applied. The structure was solved by direct methods (SIR92) and expanded using Fourier techniques (DIRDIF99). The non-hydrogen atoms except for some water O atoms were refined anisotropically by full-matrix least-squares methods. Hydrogen atoms except those of water molecules were placed at calculated positions but were not refined. All calculations were performed using the CrystalStructure crystallographic software package except for refinement, which was performed using SHELXL-97. Three ordered (Rh1-Rh3) and a half of disordered (Rh4) complex cations were crystallographically independent. The disordered cation (Rh4) lies on a crystallographic C_2-axis, and the occupancy factors of all atoms in the complex cation (Rh4) were fixed to 0.5. Four DFIX restraints [(d_{C-C}) = 1.50(1) Å and (d_{C-N}) = 1.48(1) Å] and EADP (C61-C66) constraints were used to model three N,S-chelate rings in the disordered cation. Two phenyl rings in the disordered cation (Rh4) were fixed using on AFIX 66 restraint. Several chrolide anions (Cl6-Cl9) and water solvents (O4-O21) were disordered.

Single crystal X-ray diffraction measurements for [**1b**]$Cl_2 \cdot H_2O$ were made on a Rigaku AFC5R four-cycle diffractometer with a graphite monochrometed Mo-Kα radiation. Unit cell parameters were determined by a least-squares refinement, using the angular setting of 25 centered reflections. The intensity data were collected by the ω-2θ scan mode up to $2\theta = 60.0°$. The intensities were collected for Lorentz and polarization. Empirical absorption corrections based on a series of Ψ scans were also applied. The 5937 independent reflections with $I > 2\sigma(I)$ of the measured 7285 reflections were considered as "observed" and used for the structure determination ($R_{int} = 0.016$). The structures were solved by direct methods (SIR92) and expanded using Fourier techniques (DIRDIF99). The non-hydrogen atoms were refined anisotropically by full-matrix least squares methods. Hydrogen atoms were treated independently except for C-H hydrogen atoms, which were treated by constrained refinement. All calculations were performed using the CrystalStructure crystallographic software package except for refinement, which was performed using SHELXL-97.

Table S1. Absorption and CD spectra of $\Lambda RR(R_{ax})$-[Rh(aet)(L)]$^{2+}$ ($(+)^{CD}_{330}$-[**1a**]$^{2+}$), $\Delta SS(S_{ax})$-[Rh(aet)(L)]$^{2+}$ ($(-)^{CD}_{330}$-[**1a**]$^{2+}$), $\Lambda RR(S_{ax})$-[Rh(aet)(L)]$^{2+}$ ($(+)^{CD}_{330}$-[**1b**]$^{2+}$), and $\Delta SS(R_{ax})$-[Rh(aet)(L)]$^{2+}$ ($(-)^{CD}_{330}$-[**1b**]$^{2+}$) in H_2O. (sh = shoulder)

Abs maxima: $\sigma/10^3$ cm^{-1} (log ε/mol^{-1} dm^3 cm^{-1})	
$\Lambda RR(R_{ax})/\Delta SS(S_{ax})$-[Rh(aet)(L)]$^{2+}$ ([**1a**]$^{2+}$)	
23.2	(2.22)sh
29.7	(2.77)sh
36.6	(3.69)sh
45.8	(4.60)
$\Lambda RR(S_{ax})/\Delta SS(R_{ax})$-[Rh(aet)(L)]$^{2+}$ ([**1b**]$^{2+}$)	
23.4	(2.24)
30.2	(2.94)sh
36.1	(3.58)sh
41.2	(4.37)sh

CD extrema: $\sigma/10^3$ cm^{-1} ($\Delta\varepsilon$/mol^{-1} dm^3 cm^{-1})			
$\Lambda RR(R_{ax})$-[Rh(aet)(L)]$^{2+}$ ($(+)^{CD}_{330}$-[**1a**]$^{2+}$)		$\Delta SS(S_{ax})$-[Rh(aet)(L)]$^{2+}$ ($(-)^{CD}_{330}$-[**1a**]$^{2+}$)	
24.2	(– 0.5)	24.2	(+ 0.5)
30.1	(+ 12.0)	30.2	(– 12.0)
35.1	(– 6.1)	35.0	(+ 6.1)
37.3	(+ 0.7)	36.5	(– 1.2)
40.3	(– 10.3)	40.0	(+ 9.4)
44.3	(– 23.6)	44.4	(+ 22.3)
$\Lambda RR(S_{ax})$-[Rh(aet)(L)]$^{2+}$ ($(+)^{CD}_{330}$-[**1b**]$^{2+}$)		$\Delta SS(R_{ax})$-[Rh(aet)(L)]$^{2+}$ ($(-)^{CD}_{330}$-[**1b**]$^{2+}$)	
23.4	(+ 1.1)	23.7	(– 1.1)
30.7	(+ 18.8)	30.7	(– 18.8)
35.6	(+ 4.9)	35.6	(– 4.6)
36.8	(+ 4.4)	36.7	(– 4.1)
41.2	(+ 22.8)	41.2	(– 22.0)

Table S2. Crystallographic data of Δ*SS*(S_{ax})/Λ*RR*(R_{ax})-[Rh(aet)(L)]Cl_2·4.35H_2O ([**1a**]Cl_2·4.35H_2O) and Δ*SS*(R_{ax})/Λ*RR*(S_{ax})-[Rh(aet)(L)]Cl_2·H_2O ([**1b**]Cl_2·H_2O).

	[**1a**]Cl_2·4.35H_2O	[**1b**]Cl_2·H_2O
Empirical formula	C_{20} $H_{48.7}Cl_2N_3O_{4.35}RhS_3$	$C_{20}H_{32}Cl_2N_3ORhS_3$
Fw	670.91	600.48
Crystal color, habit	orange, plate	orange, block
Crystal size, mm	0.40 x 0.20 x 0.05	0.35 x 0.30 x 0.25
Crystal system	monoclinic	triclinic
Space group	$P2_1/a$	P-1
a, Å	18.478(3)	9.6465(18)
b, Å	22.337(4)	10.9607(17)
c, Å	24.275(3)	12.3005(14)
α, °		83.776(12)
β, °	99.449(6)	75.004(14)
γ, °		86.571(12)
V, Å^3	9884(3)	1248.2(3)
Z	14	2
T, K	150(2)	296(2)
Radiation λ, Å	0.71075	0.71069
ρ_{calcd}, g cm^{-3}	1.578	1.598
μ(Mo Kα) cm^{-1}	10.49	11.67
Goodness-of-fit on F^2	1.020	1.027
$R1$[a)] [$I > 2\sigma(I)$]	0.079	0.024
R_w[b)] [All data]	0.205	0.060
Largest diff. peak and hole (e Å^{-3})	1.204 and -1.213	0.479 and -0.411

a) $R1 = \Sigma|(|F_o|-|F_c|)| / \Sigma(|F_o|)$.

b) $R_w = [\Sigma(w(F_o^2-F_c^2)^2 / \Sigma w(F_o^2)^2]^{1/2}$.

Table S3. Selected bond distances (Å) and angles (°) of Δ*SS*(S_{ax})/Λ*RR*(R_{ax})-[Rh(aet)(L)]Cl_2·4.35H_2O ([**1a**]Cl_2·4.35H_2O).

Rh(1)-N(3)	2.093(6)	Rh(3)-N(7)	2.081(7)
Rh(1)-N(1)	2.100(6)	Rh(3)-N(9)	2.104(7)
Rh(1)-N(2)	2.161(6)	Rh(3)-N(8)	2.158(7)
Rh(1)-S(2)	2.313(2)	Rh(3)-S(8)	2.299(2)
Rh(1)-S(3)	2.313(2)	Rh(3)-S(7)	2.324(2)
Rh(1)-S(1)	2.3245(17)	Rh(3)-S(9)	2.328(2)
Rh(2)-N(6)	2.087(5)	Rh(4)-N(10)	2.094(16)
Rh(2)-N(4)	2.091(6)	Rh(4)-N(12)	2.103(16)
Rh(2)-N(5)	2.140(5)	Rh(4)-N(11)	2.188(19)
Rh(2)-S(6)	2.3237(18)	Rh(4)-S(10)	2.305(5)
Rh(2)-S(5)	2.3258(17)	Rh(4)-S(11)	2.306(5)
Rh(2)-S(4)	2.3306(17)	Rh(4)-S(12)	2.339(8)
N(3)-Rh(1)-N(1)	90.5(3)	N(7)-Rh(3)-N(9)	90.1(3)
N(3)-Rh(1)-N(2)	89.7(3)	N(7)-Rh(3)-N(8)	91.0(3)
N(1)-Rh(1)-N(2)	91.3(2)	N(9)-Rh(3)-N(8)	90.0(3)
N(3)-Rh(1)-S(2)	84.2(3)	N(7)-Rh(3)-S(8)	173.8(2)
N(1)-Rh(1)-S(2)	173.37(19)	N(9)-Rh(3)-S(8)	84.9(2)
N(2)-Rh(1)-S(2)	84.69(18)	N(8)-Rh(3)-S(8)	85.4(2)
N(3)-Rh(1)-S(3)	86.3(2)	N(7)-Rh(3)-S(7)	86.1(2)
N(1)-Rh(1)-S(3)	89.70(18)	N(9)-Rh(3)-S(7)	175.3(2)
N(2)-Rh(1)-S(3)	175.89(18)	N(8)-Rh(3)-S(7)	87.4(2)
S(2)-Rh(1)-S(3)	93.89(8)	S(8)-Rh(3)-S(7)	98.78(8)
N(3)-Rh(1)-S(1)	176.1(2)	N(7)-Rh(3)-S(9)	91.0(3)
N(1)-Rh(1)-S(1)	85.90(17)	N(9)-Rh(3)-S(9)	85.7(2)
N(2)-Rh(1)-S(1)	88.85(17)	N(8)-Rh(3)-S(9)	175.3(2)
S(2)-Rh(1)-S(1)	99.31(7)	S(8)-Rh(3)-S(9)	92.30(9)
S(3)-Rh(1)-S(1)	95.20(7)	S(7)-Rh(3)-S(9)	96.95(8)
N(6)-Rh(2)-N(4)	89.5(2)	N(10)-Rh(4)-N(12)	88.4(7)
N(6)-Rh(2)-N(5)	89.3(2)	N(10)-Rh(4)-N(11)	95.4(7)
N(4)-Rh(2)-N(5)	90.3(2)	N(12)-Rh(4)-N(11)	92.0(8)
N(6)-Rh(2)-S(6)	86.10(16)	N(10)-Rh(4)-S(10)	87.0(5)
N(4)-Rh(2)-S(6)	91.95(17)	N(12)-Rh(4)-S(10)	175.0(4)
N(5)-Rh(2)-S(6)	174.80(14)	N(11)-Rh(4)-S(10)	86.5(6)
N(6)-Rh(2)-S(5)	84.51(16)	N(10)-Rh(4)-S(11)	172.8(5)
N(4)-Rh(2)-S(5)	172.39(16)	N(12)-Rh(4)-S(11)	84.5(5)
N(5)-Rh(2)-S(5)	84.92(14)	N(11)-Rh(4)-S(11)	83.3(5)
S(6)-Rh(2)-S(5)	92.30(7)	S(10)-Rh(4)-S(11)	99.98(19)
N(6)-Rh(2)-S(4)	174.73(16)	N(10)-Rh(4)-S(12)	88.7(6)
N(4)-Rh(2)-S(4)	85.28(16)	N(12)-Rh(4)-S(12)	87.1(6)
N(5)-Rh(2)-S(4)	90.13(14)	N(11)-Rh(4)-S(12)	175.8(5)
S(6)-Rh(2)-S(4)	94.71(6)	S(10)-Rh(4)-S(12)	94.7(3)
S(5)-Rh(2)-S(4)	100.66(6)	S(11)-Rh(4)-S(12)	92.5(2)

Table S4. Selected bond distances (Å) and angles (°) of Δ*SS*(R_{ax})/Λ*RR*(S_{ax})-[Rh(aet)(L)]Cl_2·H_2O ([**1b**]Cl_2·H_2O).

Rh(1)-N(3)	2.0995(17)	Rh(1)-S(2)	2.3125(6)
Rh(1)-N(1)	2.0999(18)	Rh(1)-S(3)	2.3204(6)
Rh(1)-N(2)	2.1547(18)	Rh(1)-S(1)	2.3291(6)
N(3)-Rh(1)-N(1)	90.61(7)	N(2)-Rh(1)-S(3)	85.80(5)
N(3)-Rh(1)-N(2)	93.92(7)	S(2)-Rh(1)-S(3)	96.43(2)
N(1)-Rh(1)-N(2)	94.51(8)	N(3)-Rh(1)-S(1)	88.72(6)
N(3)-Rh(1)-S(2)	177.40(5)	N(1)-Rh(1)-S(1)	84.41(6)
N(1)-Rh(1)-S(2)	87.62(6)	N(2)-Rh(1)-S(1)	177.16(5)
N(2)-Rh(1)-S(2)	84.33(5)	S(2)-Rh(1)-S(1)	92.99(2)
N(3)-Rh(1)-S(3)	85.34(5)	S(3)-Rh(1)-S(1)	95.47(2)
N(1)-Rh(1)-S(3)	175.95(6)		

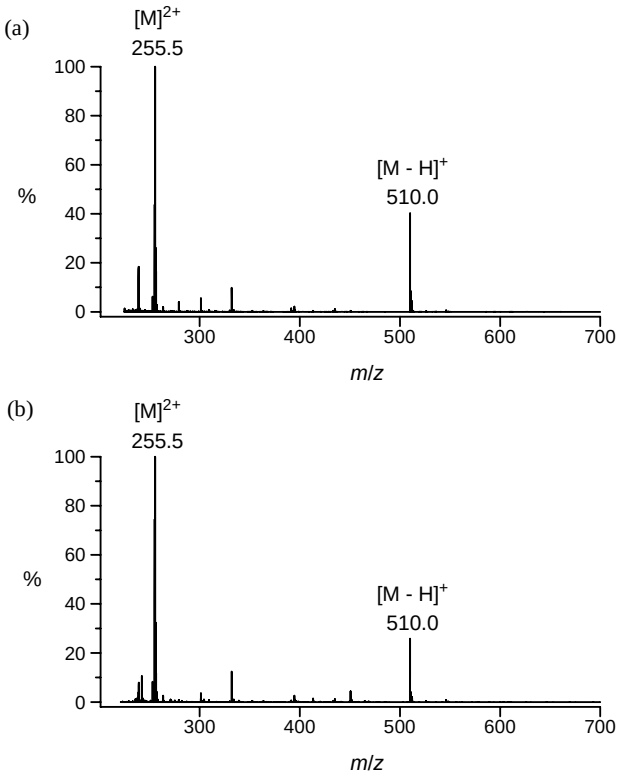

Figure S1. ESI mass spectra of Δ*SS*(*S*ax)/Λ*RR*(*R*ax)-[Rh(aet)(L)]Cl_2·5H_2O ([**1a**]Cl_2·5H_2O) (a) and Δ*SS*(*R*ax)/Λ*RR*(*S*ax)-[Rh(aet)(L)]Cl_2·H_2O ([**1b**]Cl_2·H_2O) (b) in MeOH/H_2O. The symbol 'M' denotes the complex cation of each compound.

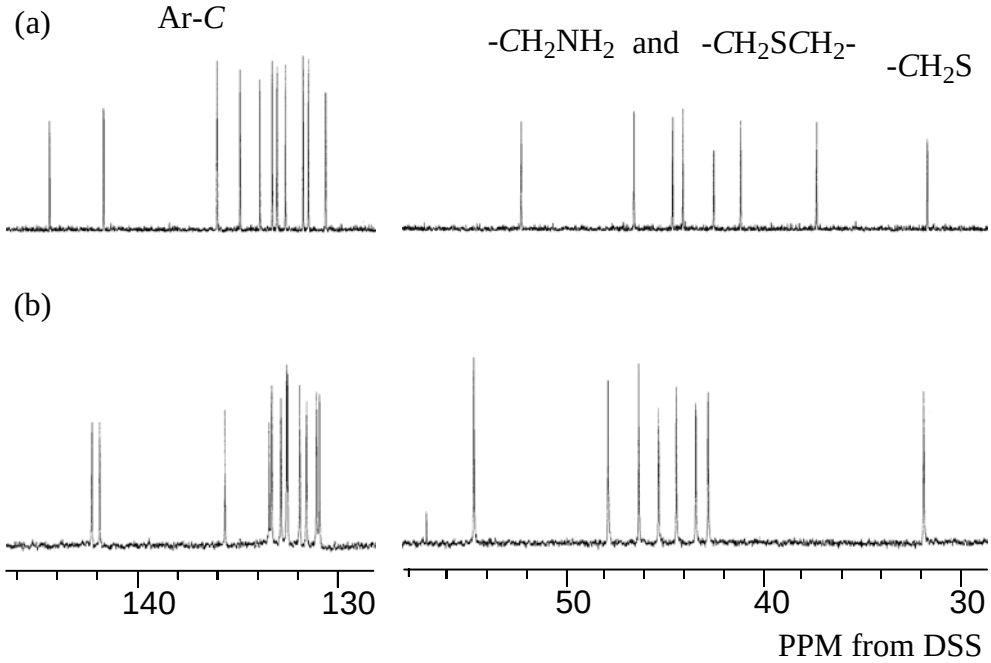

Figure S2. $^{13}C\{^1H\}$ NMR spectra of Δ*SS*(*S*ax)/Λ*RR*(*R*ax)-[Rh(aet)(L)]$^{2+}$ ([**1a**]$^{2+}$) (a) and Δ*SS*(*R*ax)/Λ*RR*(*S*ax)-[Rh(aet)(L)]$^{2+}$ ([**1b**]$^{2+}$) (b) in D_2O.

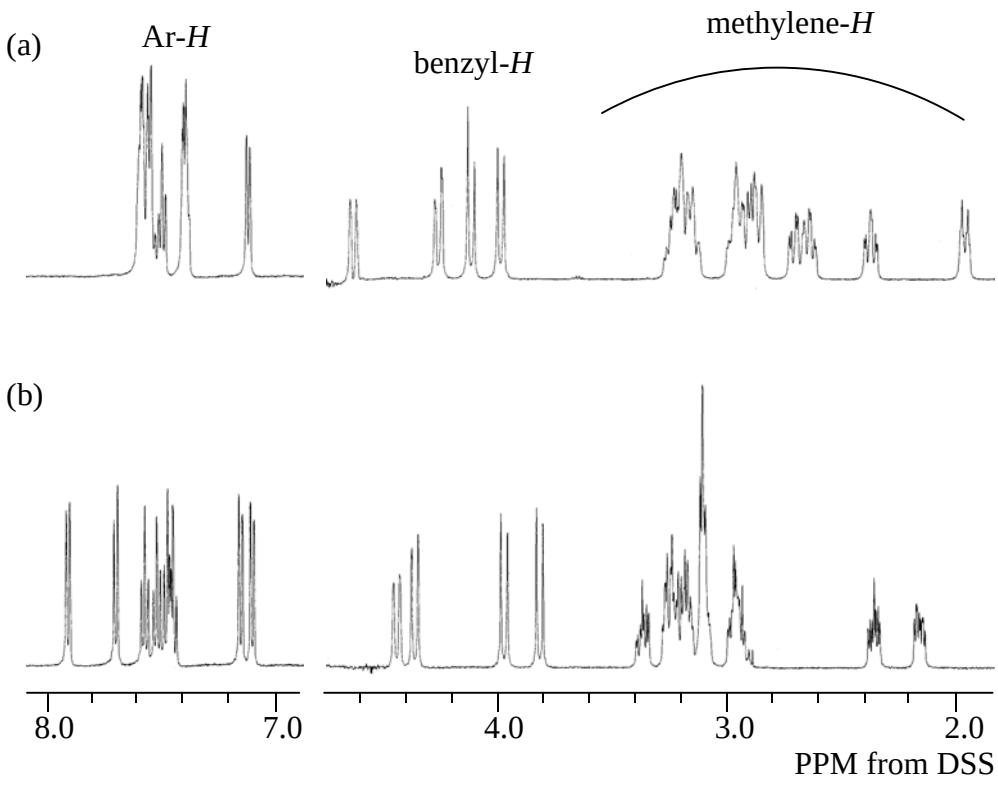

Figure S3. ^{1}H NMR spectra of Δ*SS*(S_{ax})/Λ*RR*(R_{ax})-[Rh(aet)(L)]$^{2+}$ ([**1a**]$^{2+}$) (a) and Δ*SS*(R_{ax})/Λ*RR*(S_{ax})-[Rh(aet)(L)]$^{2+}$ ([**1b**]$^{2+}$) (b) in D_2O.

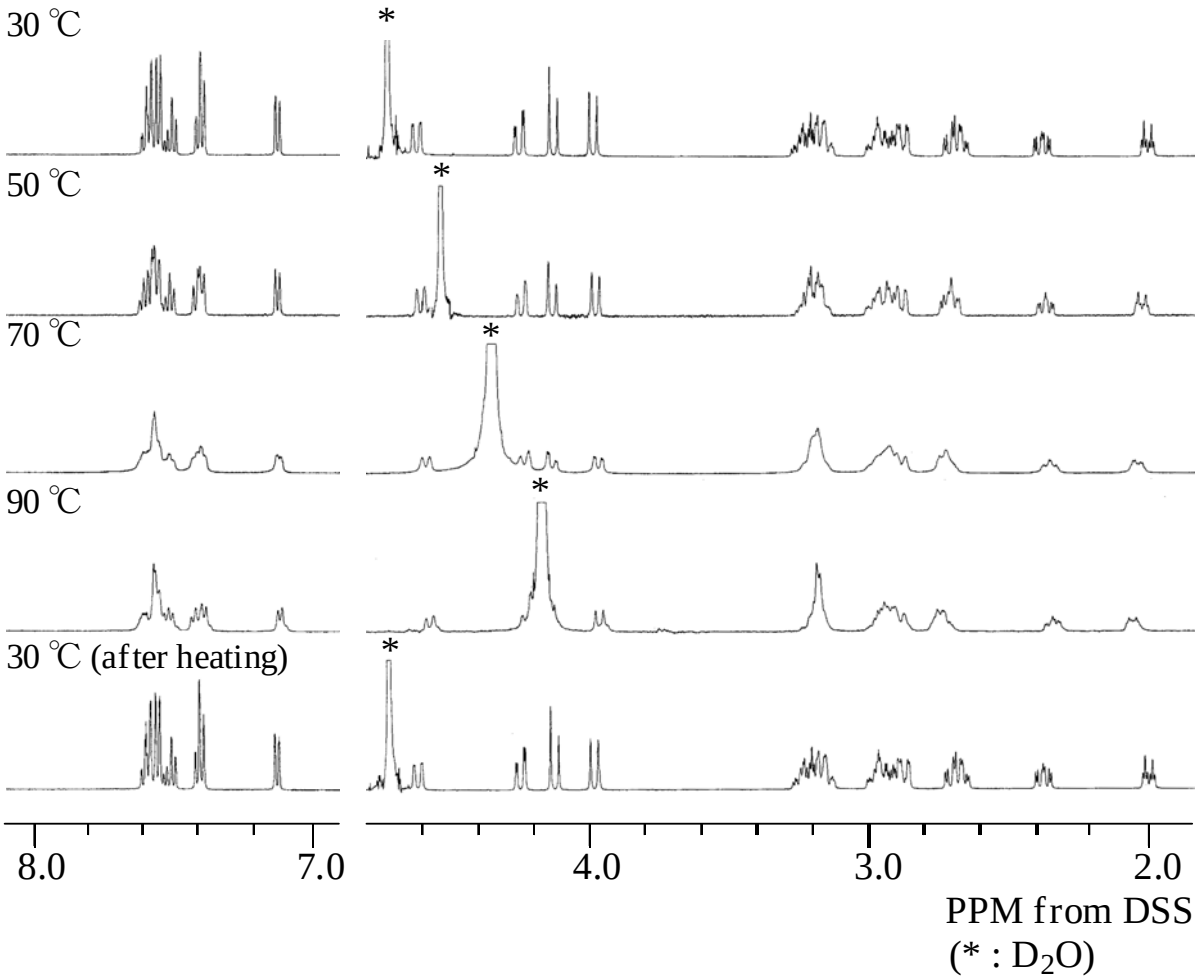

Figure S4. VT ^{1}H NMR spectra of Δ*SS*(S_{ax})/Λ*RR*(R_{ax})-[Rh(aet)(L)]$^{2+}$ ([**1a**]$^{2+}$) in D_2O. The spectra were recorded every 25 min from 30°C to 90°C. The spectrum at 30°C after heating is identical with that before heating.

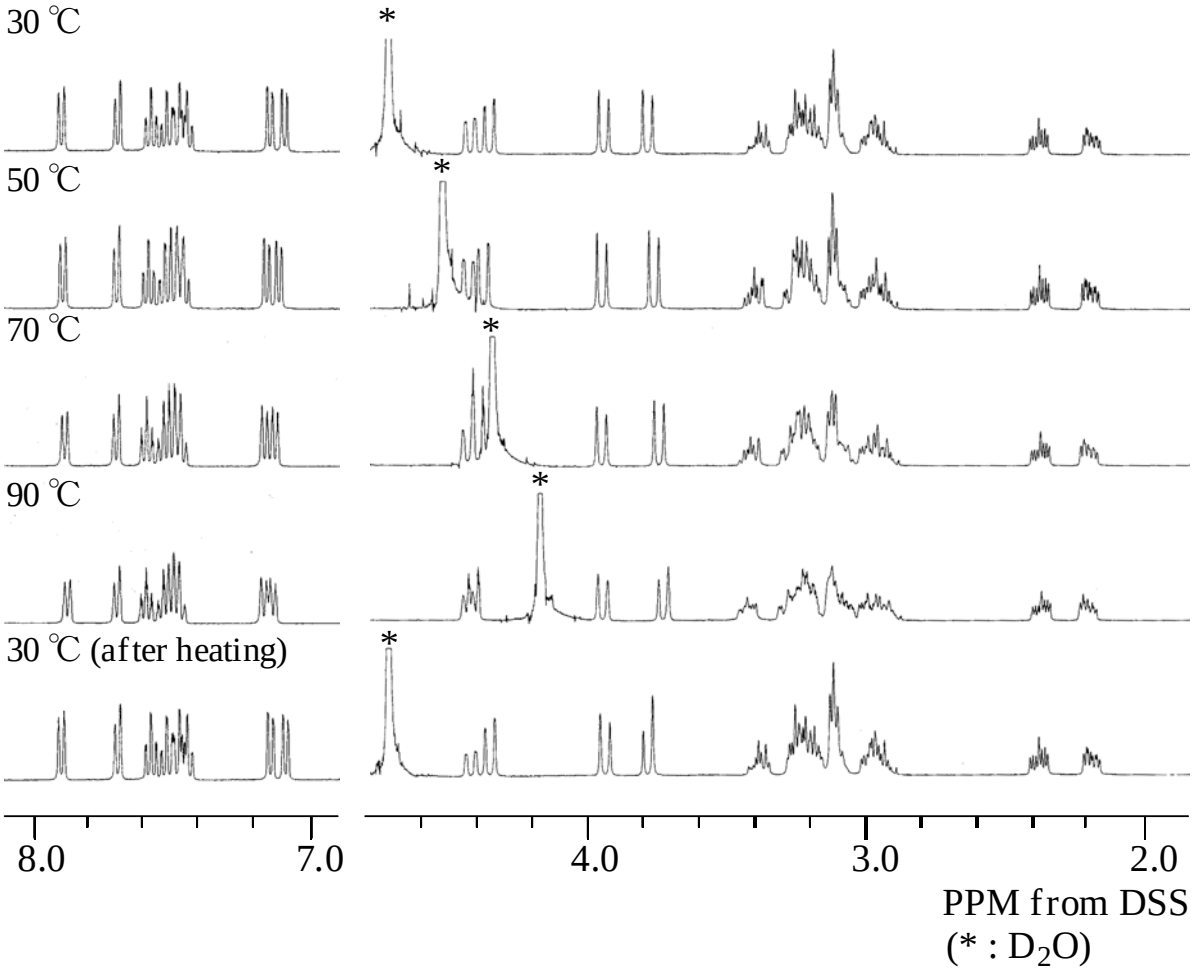

Figure S5. VT ^{1}H NMR spectra of Δ*SS*(R_{ax})/Λ*RR*(S_{ax})-[Rh(aet)(L)]$^{2+}$ ([**1b**]$^{2+}$) in D_2O. The spectra were recorded every 25 min from 30°C to 90°C. The spectrum at 30°C after heating is identical with that before heating.

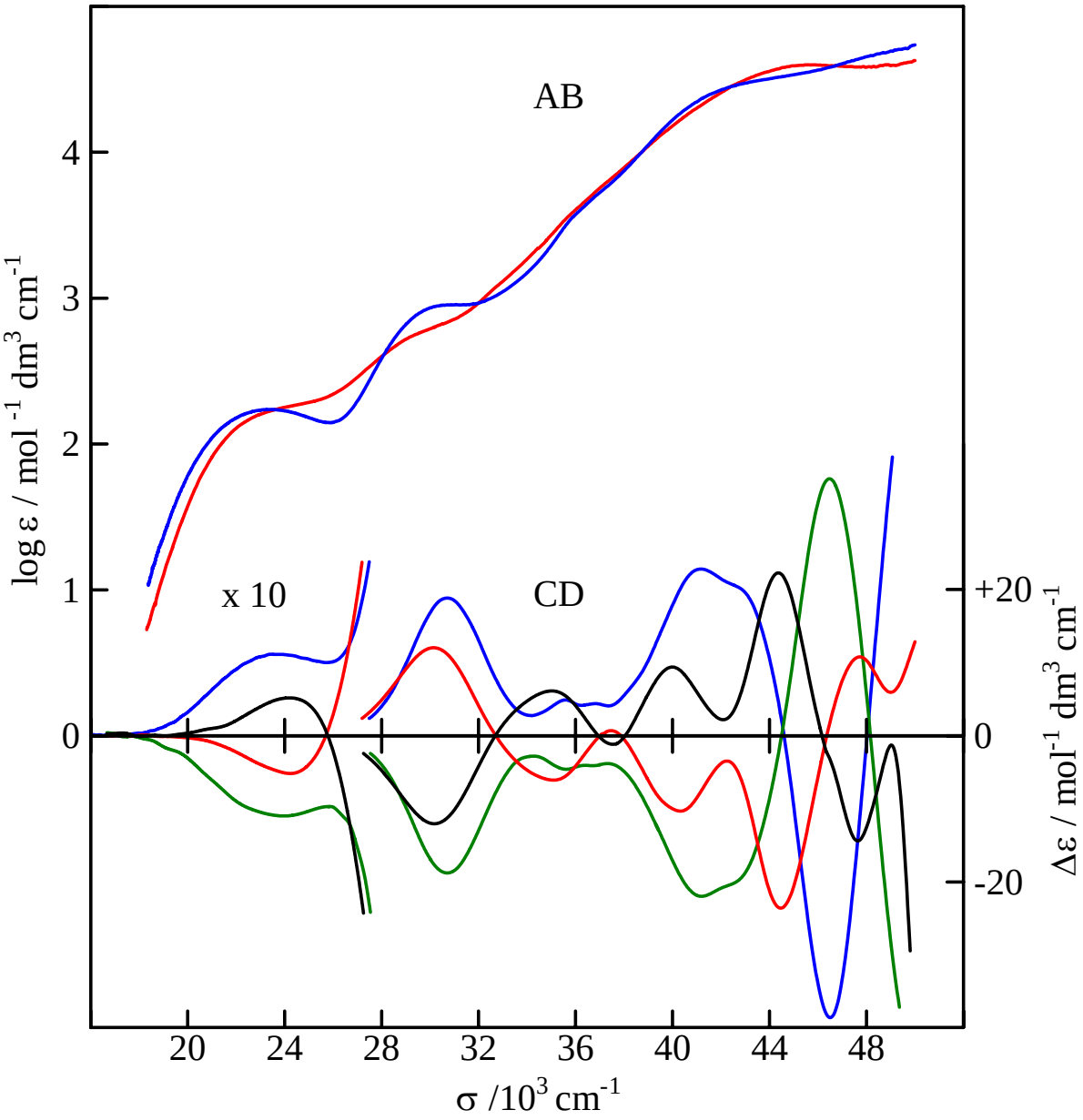

Figure S6. Absorption and CD spectra of Λ*RR*(R_{ax})-[Rh(aet)(L)]$^{2+}$ ((+)$^{CD}_{330}$-[**1a**]$^{2+}$) (—), Δ*SS*(S_{ax})-[Rh(aet)(L)]$^{2+}$ ((−)$^{CD}_{330}$-[**1a**]$^{2+}$) (—), Λ*RR*(S_{ax})-[Rh(aet)(L)]$^{2+}$ ((+)$^{CD}_{330}$-[**1b**]$^{2+}$), (—) and Δ*SS*(R_{ax})-[Rh(aet)(L)]$^{2+}$ ((−)$^{CD}_{330}$-[**1b**]$^{2+}$) (—) in H_2O.